Bathymetry and Atomic Gravimetry Sensor Fusion for Autonomous Underwater Vehicle

Camille Palmier, Karim Dahia, Nicolas Merlinge, Dann Laneuville, Pierre Del Moral

Bathymetry and Atomic Gravimetry Sensor Fusion for Autonomous Underwater Vehicle

Camille Palmier[1], Karim Dahia[1], Nicolas Merlinge[1],
Dann Laneuville[2] and Pierre Del Moral[3]
[1] ONERA - The French Aerospace Lab [2] Naval Group [3] INRIA

***Abstract*—Terrain-aided navigation provides a drift-free navigation approach for autonomous underwater vehicles. However, velocity is often tricky to estimate with conventional bathymetry (mono or multi-beam telemetry) sensors. Cold atom gravimetry is a promising absolute and autonomous additional sensor that is seldom considered for this kind of application. We investigate a multi-beam telemeter and gravimeter centralized fusion scenario and the resulting observability gain on velocity. To do so, an Adaptive Approximate Bayesian Computation Regularized Particle Filter is implemented and compared to conventional Regularized Particle Filter. Numerical results are presented and the robustness of the bathymetry and gravimetry fusion strategy is demonstrated, yielding less non-convergence cases and more accurate position and velocity estimation.**

I. Introduction

The autonomy of underwater vehicles is a broad and extensive field of study [2]. The autonomy depends on the ability to perform long-term and long-range missions without the need for human intervention. The navigation of Autonomous Underwater Vehicles (AUV [2]) is often based on Inertial Measurements Unit (IMU). Although IMU are autonomous and reliable, they provide imperfect measurements (e.g., subject to bias, noises) that result a drifting error in the navigation solution. To correct the navigation drift, IMU can be combined with other external sensors. A common aiding source is the Global Positioning System (GPS) but resurfacing for GPS is often excluded for discretion requirements and also because it can easily be jammed. This is especially true for military-grade AUVs. Terrain Aided Navigation (TAN) provides a drift-free navigation tool for underwater operations. TAN aims to retrieve the vehicle current state (e.g., position or velocity) by matching a terrain profile obtained from a sensor with a profile reconstructed from an embedded map of the operation area.

Usually, the multi-beam telemeter is used for underwater navigation applications [2], [18]. This sensor provides a series of depth measurements along the AUV trajectory. In the past few years, another technology was introduced: the atomic gravimeter. The atomic gravimeter is a promising absolute sensor for underwater navigation. In particular, the quantum gravimetry concept developed by ONERA (cold atom gravimeter [3]) provides an absolute and accurate gravity measurement. The atomic gravimeter is starting to be used in underwater navigation [16] but, to the best of the authors knowledge, has not been combined with other TAN sensors.

Performing sensor fusion makes it necessary to resort to robust nonlinear filtering algorithms. State estimation problem is particularly challenging for TAN applications. Indeed, the use of embedded maps involves severe measurement ambiguities (i.e. when a measurement may correspond to several areas on the map). In the presence of strong nonlinearities and multi-modality due to terrain map ambiguities, the Extended Kalman Filter (EKF [4]) is known to be unreliable. The linearization of terrain areas where abrupt changes in seabed elevation occur generates numerical instabilities that may result in estimation divergence. In order to avoid linearization, several stochastic filters were proposed such as the Particle Filter (a.k.a. Monte Carlo methods [5]).

The idea of this paper is to improve the AUV state estimation by fusing the classic multi-beam telemeter with a gravimeter. The fusion is performed by an Adaptive Approximate Bayesian Computation Particle Filters (A2BC-PF, [6]). A2BC-PF are designed to tackle estimation problems where the law of the measurement noise (likelihood) is unknown. This is often the case in TAN applications that use embedded numerical terrain maps, which can lead to uncontrolled measurements errors. Maps are not exempt from uncertainty, they may not be fully representative of the field that a local sensor would measure. Furthermore, the multi-beam telemeter measurements model cannot be put into an explicit form linking the state to the measurements, which can lead to numerical approximations resulting in uncontrolled errors. In this context, neither the measurement error (involving both the sensor noise and the map modeling error), nor its probabilistic law (likelihood) can be analytically determined. The A2BC method consists of approximating the actual likelihood by a probability density kernel with an adaptive bandwidth. A2BC makes the Monte Carlo methods more robust to measurement ambiguities as the number of estimation non-convergences is significantly reduced [6].

The paper is organized as follows. The underwater terrain-aided navigation, the multi-beam telemeter and the gravimeter are introduced in Section II. Section III states the estimation problem formulation and the sensor fusion methodology. Two particle filters schemes are introduced to perform the sensor fusion. Section IV illustrates the performance of multi-beam and gravimeter fusion applied to underwater TAN. Section V concludes the paper.

II. Underwater Terrain-Aided Navigation

Autonomous underwater vehicles (AUV) need to navigate without resurfacing to correct their drifting IMU navigation solution. Therefore, IMU needs to be hybridized with one or several additional sensors to bring position-related information into the system.

Multi-beam telemeter is a widely used underwater sensor. If the terrain contains sufficient information, this sensor can be used to retrieve the state of the vehicle using an embedded numerical seabed map (see, Section II-A and Fig. 2). Although multi-beam telemeter aided navigation is able to accurately retrieve the AUV position, the velocity is often challenging to be precisely estimated. In order to enhance the accuracy of velocity estimation, we propose to fuse the multi-beam telemeter measurements with an atomic gravimeter (see Section II-B).

The atomic gravimeter is a promising absolute sensor for underwater navigation. It provides an absolute and accurate gravity measurement. The gravimeter is associated with a gravity anomalies map (see Fig. 3a).

Multi-beam telemeter and gravimeter sensors, as well as the resulting measurements equations, are described in Sections II-A and II-B respectively.

A. Multi-Beam telemeter

The multi-beam telemeter provides a series of depth measurements along the AUV position (see Fig. 1).

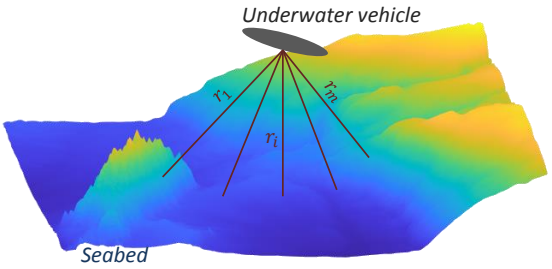

Fig. 1: Multi-beam telemeter scheme.

At each time-step, the telemeter measurements are comprised of m distances between the AUV and the seabed, which correspond to the number of beams. The measurements vector is given by:

$$y_k^b = [r_1, \dots, r_m]^\top \tag{1}$$

where r_i records the distance between the AUV and the seabed for the i-th beam. The distance equation is constructed via a projection in the Cartesian coordinate system (see Meduna [13] for details). For each beam, r_i is equal to:

$$r_i = \sqrt{(p^x - p_i^x)^2 + (p^y - p_i^y)^2 + (p^z - \text{map}_{\text{mb}}(p_i^x, p_i^y))^2} + \nu_i \tag{2}$$

where map_{mb} is the bathymetric map of the operation area (see Fig. 2) and ν_i is the measurements white noise of covariance R^b. The bathymetric map is a nonlinear function of $\mathbb{R}^2$ in $\mathbb{R}$, taking as input the position in axis x and y and giving as output the elevation of the terrain. The range r_i is computed by determining the intersection point of the inertial beam direction vector with the terrain $p_i = [p_i^x, p_i^y, p_i^z]^\top$ where $p_i^z = \text{map}_{\text{mb}}(p_i^x, p_i^y)$ (see Fig. 3.4 in [13]). As the intersection point is unknown in practice, the multi-beam telemeter measurements equation (1) is computed through numerical approximations (e.g., via grid search methods). The measurements noise accounts for these approximations in addition to sensor and map errors. However, as the numerical approximations introduce some unknown sampling noise that are difficult to control, the law of the measurements noise is complex to infer.

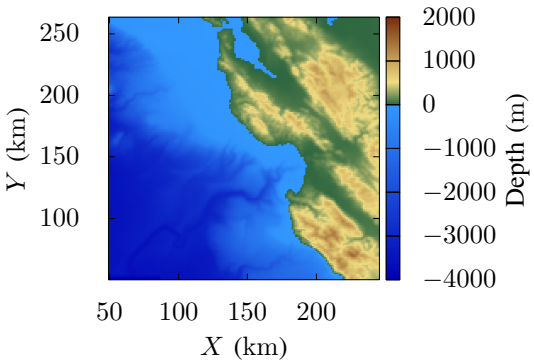

Fig. 2: Bathymetric map of the California coast (35°51′ N, 121°27′ W). The colorbar represents the depth levels (m).

B. Atomic gravimeter

The atomic gravimeter measures the absolute value of the gravity by monitoring the free-fall acceleration of ultra-cold atoms thanks to atom interferometry [14], [15]. The measurements are absolute and accurate, which means that the sensors does not need any calibration and provides a gravity evaluation with a very low level noise (on the order of 10^{-2} mGal, where 1 mGal is equal to 10^{-5} m s^{-2}).

The gravimeter measurements equation is obtained from the vertical acceleration model expressed in the earth-centered earth-fixed coordinate system [16]. The vertical acceleration of the vehicle is neglected as the AUV follows a uniform rectilinear trajectory in our application. To adapt the gravimeter measurements equation to the flat Earth frame, the Eötvös effect (also known as Coriolis effect) and the nominal gravitational acceleration are linearized around a reference geographical point of the map $[\lambda = 35.5°N, \phi = 124°W, h = 0 \text{ m}]$. The equation expressed in the flat Earth frame is given by:

$$y_k^g = a\ p_k^y + b\ p_k^z + c\ v_k^x + \text{map}_{\text{ga}}(p_k^x, p_k^y) + \nu_k{}' \tag{3}$$

where map_{ga} is the gravity anomalies map (see Fig. 3a) and $\nu_k{}'$ is the measurements white noise of covariance R^g. The measurements equation y_k is expressed in mGal. The map is a nonlinear function of $\mathbb{R}^2$ in $\mathbb{R}$, taking as input the position in axis x and y in meters and giving as output the gravity anomalies in mGal. The measurements noise $\nu_k{}'$ includes sensor errors. The constants a, b and c in (3) are equal to 7.66×10^{-4} mGal, -0.3086 mGal, and 3.0542 mGal respectively. The terms $a\,p_k^y + b\,p_k^z$ and $c\,v_k^x$ represent respectively the standard gravity and the Eötvös effect.

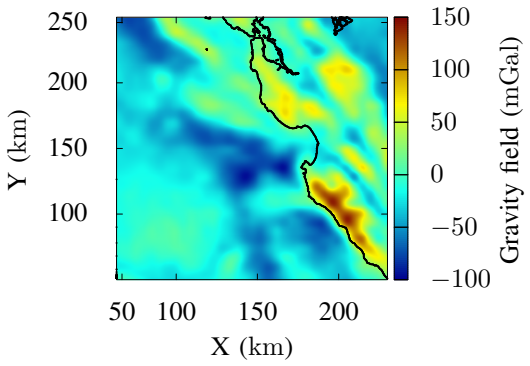

(a) Gravimetric map. The colorbar represents the gravity anomalies in (mGal)

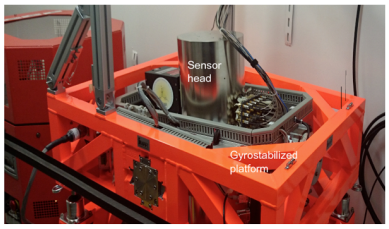

(b) Cold atom gravimeter GIRAFE 2 and its gyrostabilizing platform.

Fig. 3: Gravimetric map of the Californian coasts (35°51′ N, 121°27′ W) and quantum gravimeter.

The gravimeter-based navigation does not allow an accurate estimation of the position of the AUV because of the poor resolution of the gravity anomalies maps. However, it allows a better estimation of the velocity than the telemeter-based navigation as the velocity in the x-axis is directly observable in the measurements equation (3).

III. Estimation problem and sensor fusion architecture

TAN navigation is related to a state estimation problem. We consider the following discrete-time dynamical model with hidden states $\{x_k\}_{k\geq 0} \in \mathbb{R}^d$ and measurements $\{y_k\}_{k\geq 1} \in \mathbb{R}^{d_y}$:

$$\begin{cases} x_k = f_k(x_{k-1}) + \eta_k \\ y_k = h_k(x_k) + v_k \end{cases} \tag{4}$$

where f_k and h_k are respectively the dynamical model and the measurements function, and η_k and v_k respectively the process noise and measurements noise. Noises are independent and identically distributed (i.i.d.), mutually independent and independent of the initial state x_0.

The state x_k corresponds to the vehicle state (e.g. position, velocity). The measurements equation can be for example the multi-beam telemeter equation (1).

A. Filtering framework

Bayesian filters aim to estimate the posterior density of the state variables at the time k given the past measurements. State estimation consists of two steps: prediction and correction.

- The prediction step determines a prior density $p(x_k|y_{1:k-1})$ with respect to the transition density $p(x_k|x_{k-1})$ and the previous posterior density $p(x_{k-1}|y_{1:k-1})$ via the Chapman-Kolmogorov equation:

$$p(x_k|y_{1:k-1}) = \int p(x_k|x_{k-1})\ p(x_{k-1}|y_{1:k-1})\ dx_{k-1} \tag{5}$$

- The correction step determines the posterior density of the state with respect to the prior density (5) and the likelihood $p(y_k|x_k)$. From Bayes' law, one obtains:

$$p(x_k|y_{1:k}) = \frac{p(y_k|x_k)\ p(x_k|y_{1:k-1})}{\int p(y_k|x_k)\ p(x_k|y_{1:k-1})\ dx_k} \tag{6}$$

If the state and the measurements functions are linear, the process and measurements noises are Gaussian, and the initial density p_0 is Gaussian then the Kalman filter provides an optimal analytic iterative formulation of the posterior density. The Kalman formulation was extended to nonlinear models, but it is not robust to severe nonlinearities and non-Gaussian densities. For highly nonlinear models, several methods based on Monte Carlo sampling of the filtering law were proposed to approximate the posterior density.

Two particle filters are presented in the next sections: the Regularized Particle Filter (RPF) and the Adaptive Approximate Bayesian Computation - Regularized Particle Filter (A2BC-RPF). The RPF is based on kernel estimation approaches which brings more accuracy by considering mixtures of weighted bounded kernels. The A2BC-RPF is based on Approximate Bayesian Computation (ABC) methods which enables to handle cases where the law of the measurements noise is unknown. This is the case for the bathymetric-based navigation as discussed in Section II-A. Indeed, the law of the measurements noise is difficult to infer as the measurements equation is derived from numerical approximations.

B. Regularized Particle Filter

The RPF [1] approximates the empirical state density of the conventional particle filter with a smoothed density. The purpose of regularization is to ensure that the assumption of samples independence is respected by injecting an optimally designed noise to the signal. The posterior density can be rewritten as a mixture of weighted kernels:

$$p(x_k|y_{1:k}) \approx \sum_{i=1}^{N} w_k^i \mathcal{K}_h(x_k - x_k^i) \tag{7}$$

where N is the number of state samples called particles, $(x_k^i)_{i=1,\dots,N}$ are the particles, and $(w_k^i)_{i=1,\dots,N}$ are the associated weights such that $\sum_{i=1}^{N} w_k^i = 1$. The RPF equations are described in Algorithm 1. During the resampling step, the particles x_k^i with high normalized weights w_k^i are selected and low-weighted particles are discarded. The selected particles are duplicated according to their weights in order to keep a constant total number of particles. The new set of particles is called x_k^i and the weights are set such that $w_k^i = 1/N$. The resampling is used to decrease the weight variance and

Algorithm 1 RPF

Initialization: For $i = 1, \dots, N$, initialize the particles $x_0^i \sim p_0(x_0)$ from a prior distribution and set $w_0^i = 1/N$.
for k = 1, 2, ... **do**
- [Prediction:] Sample the particles using the transition density: $\forall i,\ x_k^i \sim p(x_k|x_{k-1}^i)$.
- [Correction:] Update the weights $\forall i$, $\tilde{w}_k^i = w_{k-1}^i\ p(y_k|x_k^i)$ and normalized $w_k^i = \tilde{w}_k^i / \sum_i \tilde{w}_k^i$.
- [Estimation:] Compute the state estimate $\hat{x}_k = \sum_{i=1}^N w_k^i\, x_k^i$ and its covariance $\hat{P}_k = \sum_{i=1}^N \left(x_k^i - \hat{x}_k\right)\left(x_k^i - \hat{x}_k\right)^\top$.
- [Regularized resampling:]

if $\widetilde{N}_{\mathit{eff},k}(\varepsilon) < N_{\text{th}}$ **then**
Apply some resampling procedure as described in Subsection III-B. Set $w_k^i = 1/N$. Add the regularization routine described in [1] using the optimal kernel (9) and the optimal bandwidth (10a).
end if
end for

avoids degeneracy (i.e., when a single weight tends to unity and all the others tend to zero). See [7] or [8] for a survey on resampling methods. In practice, resampling is triggered by monitoring a criterion such as the approximate efficiency [9], [10]:

$$\hat{N}_{\mathit{eff},k} = \frac{1}{\sum_{i=1}^N \left(w_k^i\right)^2} \tag{8}$$

The resampling is triggered whenever $\hat{N}_{\mathit{eff},k} < N_{\text{th}}$ where N_{th} is a given threshold.

When all particles have the same weight (it is the case immediately after the resampling step), the optimal kernel $\mathcal{K}$ is the Epanechnikov kernel [1] where the optimal bandwidth parameter h minimizes the Mean Integrated Square Error criterion.

$$\mathcal{K}(x) = \begin{cases} \frac{d+2}{2c_d}\left(1 - ||x||^2\right) & \text{if} \quad ||x|| < 1 \\ 0 \quad \text{otherwise} \end{cases} \tag{9}$$

where c_d is the volume of the unit hypersphere in $\mathbb{R}^d$. The associated optimal bandwidth is:

$$h = \mu\ A(\mathcal{K})\ N^{-\frac{1}{d+4}} \tag{10a}$$

$$A(\mathcal{K}) = \left[8c_d^{-1}(d+4)(2\sqrt{\pi})^d\right]^{\frac{1}{d+4}} \tag{10b}$$

where $0 < \mu < 1$ is a parameter introduced to limit the impact of the regularization when the assumption of unimodality is not satisfied.

C. Adaptive Approximate Bayesian Computation Particle Filters

Approximate Bayesian Computation (ABC, [11], [12]) filters were introduced to tackle cases where the likelihood law is unknown. ABC methods match the measurements y_k with simulated pseudo-measurements u_k^i. The N pseudo-measurements are generated using the particles x_k^i from the prediction step and the measurements function h_k: $u_k^i = h_k(x_k^i)$. The likelihood $p(y_k|x_k)$ is approximated by a kernel $\mathcal{K}_{\varepsilon_k}$ that reflects the closeness between the actual and simulated measurements:

$$p(y_k|x_k^i) \approx \mathcal{K}_{\varepsilon_k}(y_k - u_k^i) \tag{11}$$

where $\mathcal{K}_{\varepsilon_k} : \mathbb{R}^{dm} \to \mathbb{R}$ is set by its bandwidth parameter $\varepsilon_k > 0$. The choice of the bandwidth parameter is crucial to avoid the particles degeneracy. Particles degeneracy may arise when the supports of the likelihood and prior densities do not overlap. The objective of Adaptive Approximate Bayesian Computation method (A2BC, [6]) is to expand the likelihood to increase the consistency with the prior density, as shown in Fig. 4. The bandwidth parameter is optimized online using a criterion based on the variance of the weights: the approximate efficiency (13a).

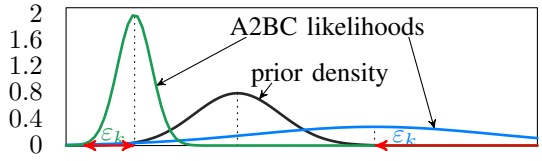

(a) Consistency between the prior density (black) and a sharp likelihood (green, $\varepsilon_k \to 0^+$) or a non-informative likelihood (blue, $\varepsilon_k \to \infty$) resulting in filter divergence or inefficient correction respectively.

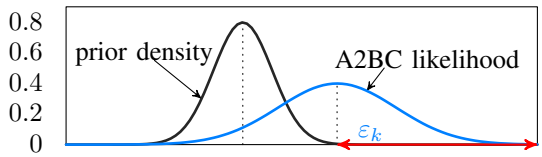

(b) Consistency between the prior density (black) and a likelihood (blue) resulting in an efficient correction.

Fig. 4: Scheme of the impact of the choice of the bandwidth parameter ε_k on the consistency between the prior density and the likelihood in the A2BC approach.

At each correction step, the bandwidth ε_k is chosen to keep the approximate efficiency above a desired value $N_{\text{th}} = \theta N$ where $0 < \theta \leq 1$ is a given threshold. The idea is to choose ε_k such that the efficiency is greater than the resampling threshold.

$$\varepsilon_k = \underset{\varepsilon \in \mathcal{D}}{\operatorname{argmin}} \left(\widetilde{N}_{\mathit{eff},k}(\varepsilon) - N_{\text{th}}\right)^2 \tag{12}$$

where $\mathcal{D} \subset \mathbb{R}^+$ is a given domain, and $\widetilde{N}_{\mathit{eff},k}(\varepsilon)$ is the approximate efficiency. The approximate efficiency (12) depends on the ABC kernel $\mathcal{K}_\varepsilon(y_k - u_k^i)$ (11) via the weights:

$$\widetilde{N}_{\mathit{eff},k}(\varepsilon) = \frac{1}{\sum_{i=1}^N \left(w_k^i(\varepsilon)\right)^2} \tag{13a}$$

$$w_k^i(\varepsilon) \propto w_{k-1}^i(\varepsilon)\, \mathcal{K}_\varepsilon(y_k - u_k^i) \tag{13b}$$

The previous optimization problem is restricted to domain $\mathcal{D}$ to access the resampling step whenever the particles are significantly misplaced.

The A2BC method can be coupled with any particle filters. In the correction step, the likelihood is replaced by its A2BC kernel approximation. The prediction and resampling steps are unchanged. In this paper, the A2BC-RPF is used and is described in Algorithm 2. The objective of A2BC is to prevent the filter from diverging by optimizing the impact of the weights correction. A significant decrease was shown in terms of non-convergences rate [6] (see Section IV-B).

Algorithm 2 A2BC-RPF

Initialization: For $i = 1, \dots, N$, initialize the particles $x_0^i \sim p_0(x_0)$ from a prior distribution and set $w_0^i = 1/N$.
for k = 1, 2, … **do**
- [Prediction:] Sample the particles using the transition density: $\forall i,\ x_k^i \sim p(x_k|x_{k-1}^i)$.
- [A2BC correction:] Compute the pseudo-measurements using the particles: $\forall i,\ u_k^i = h_k(x_k^i)$. Determine ε_k using (12). Update the weights $\forall i,\quad \tilde{w}_k^i = w_{k-1}^i \mathcal{K}_{\varepsilon_k}(y_k - u_k^i)$ and normalized $w_k^i = \tilde{w}_k^i / \sum_i \tilde{w}_k^i$.
- [Estimation:] Compute the state estimate $\hat{x}_k = \sum_{i=1}^N w_k^i x_k^i$ and its covariance $\hat{P}_k = \sum_{i=1}^N \left(x_k^i - \hat{x}_k\right)\left(x_k^i - \hat{x}_k\right)^\top$.
- [Regularized resampling:]

if $\widetilde{N}_{eff,k}(\varepsilon) < N_{\text{th}}$ **then**
Apply some resampling procedure as described in Subsection III-B. Set $w_k^i = 1/N$. Add the regularization routine described in [1] using the optimal kernel (9) and the optimal bandwidth (10a).
end if
end for

D. Sensor fusion strategy

Bathymetric and gravimetric sensor fusion by a navigation filter can be formulated as a centralized architecture, see Fig. 5. Centralized data fusion consists of designing an estimation filter able to gather information provided by the sensors and prior knowledge obtained from the dynamical and measurements models.

Performing data fusion from bathymetry and gravimetry yields several relevant advantages. Bathymetry equation (1) depends on the vehicle position and on the seabed elevation profile. The multi-beam telemeter can thus provide information explicitly depending on position. However, velocity, which is not explicitly involved in the measurement model, can only be retrieved by the filter in an indirect way. The gravity measurement equation (3) depends on geographical position and x-axis velocity. The geographical position dependency brings additional information to bathymetric data. In addition, the explicit dependency of gravity measurement equation on x-axis velocity combined with the high accuracy of the atomic sensor brings a significant observability gain.

Observability level can be quantified by the Fisher information matrix [19]. The deterministic recursive Tichavsky formulation [20] of Fisher information matrix is:

$$J^+ = H^T R^{-1} H + \left(F J^{-1} F^T + Q\right)^{-1} \tag{14}$$

where J is the prior Fisher information matrix, J^+ the posterior Fisher information matrix, F the dynamics Jacobian matrix, Q the process covariance, H the Jacobian matrix of the measurements equation and R the measurements noise covariance matrix. The two additive terms of the above equation respectively quantify the measurement and the dynamics contributions to the Fisher information matrix. For both sensor configurations (bathymetry only, or gravimetry and bathymetry fusion) the dynamics contribution is the same and allows non explicitly observed variables (e.g. velocity) to be indirectly observed by integration correlation.

Let us focus on the measurement contribution to Fisher information matrix:

$$J_m = H^T R^{-1} H \tag{15}$$

In this paragraph only, for the sake of simplicity, the bathymetry equation is approached as a single-beam telemeter pointing towards the local vertical direction:

$$y^b = p^z - \text{map}_{\text{mb}}(p^x, p^y) + v \tag{16}$$

By applying (15), the bathymetry contribution to information can then be expressed as:

$$J_{\text{bathy}} = \begin{bmatrix} \frac{(\nabla_b^x)^2}{\sigma_b^2} & \frac{\nabla_b^x \nabla_b^y}{\sigma_b^2} & -\frac{\nabla_b^x}{\sigma_b^2} & 0 & 0 & 0 \\ \frac{\nabla_b^x \nabla_b^y}{\sigma_b^2} & \frac{(\nabla_b^y)^2}{\sigma_b^2} & -\frac{\nabla_b^y}{\sigma_b^2} & 0 & 0 & 0 \\ -\frac{\nabla_b^x}{\sigma_b^2} & -\frac{\nabla_b^y}{\sigma_b^2} & \frac{1}{\sigma_b^2} & 0 & 0 & 0 \\ 0 & 0 & 0 & 0 & 0 & 0 \\ 0 & 0 & 0 & 0 & 0 & 0 \\ 0 & 0 & 0 & 0 & 0 & 0 \end{bmatrix} \tag{17}$$

where ∇_b^x and ∇_b^y are respectively the East and North gradients of the seabed elevation map ($\text{map}_{\text{mb}}(p^x, p^y)$) and σ_b is the standard deviation of the telemeter measurement error v.

By adding the gravity field measurement, the measurements equation becomes:

$$y_k = [y_k^b, y_k^g]^\top \tag{18}$$

The contribution of both sensors to information can be expressed by J_{fusion} equals to:

$$\begin{bmatrix} \frac{(\nabla_b^x)^2}{\sigma_b^2} + \frac{\left(\nabla_g^x\right)^2}{\sigma_g^2} & \frac{\nabla_b^x \nabla_b^y}{\sigma_b^2} + \frac{\nabla_g^x\left(\nabla_g^y + a\right)}{\sigma_g^2} & -\frac{\nabla_b^x}{\sigma_b^2} + \frac{\nabla_g^x b}{\sigma_g^2} & \frac{\nabla_g^x c}{\sigma_g^2} & 0 & 0 \\ \frac{\nabla_b^x \nabla_b^y}{\sigma_b^2} + \frac{\nabla_g^x\left(\nabla_g^y + a\right)}{\sigma_g^2} & \frac{(\nabla_b^y)^2}{\sigma_b^2} + \frac{\left(\nabla_g^y + a\right)^2}{\sigma_g^2} & -\frac{\nabla_b^y}{\sigma_b^2} + \frac{b\left(\nabla_g^y + a\right)}{\sigma_g^2} & \frac{c\left(\nabla_g^y + a\right)}{\sigma_g^2} & 0 & 0 \\ -\frac{\nabla_b^x}{\sigma_b^2} + \frac{\nabla_g^x b}{\sigma_g^2} & -\frac{\nabla_b^y}{\sigma_b^2} + \frac{b\left(\nabla_g^y + a\right)}{\sigma_g^2} & \frac{b^2}{\sigma_g^2} + \frac{1}{\sigma_b^2} & \frac{bc}{\sigma_g^2} & 0 & 0 \\ \frac{\nabla_g^x c}{\sigma_g^2} & \frac{c\left(\nabla_g^y + a\right)}{\sigma_g^2} & \frac{bc}{\sigma_g^2} & \frac{c^2}{\sigma_g^2} & 0 & 0 \\ 0 & 0 & 0 & 0 & 0 & 0 \\ 0 & 0 & 0 & 0 & 0 & 0 \end{bmatrix} \tag{19}$$

where ∇_g^x and ∇_g^y are respectively the East and North local gradients of the gravimetry anomaly map ($\text{map}_{\text{ga}}(p^x, p^y)$) and σ_g is the standard deviation of the atomic gravimeter measurement error.

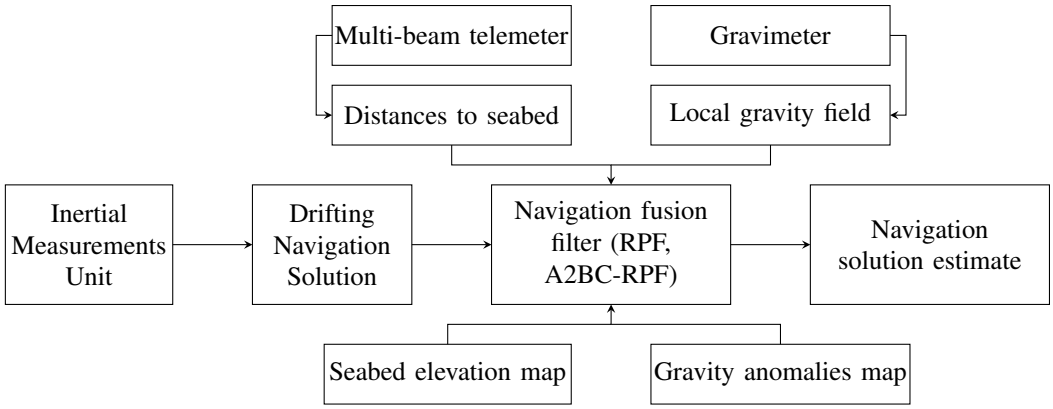

Fig. 5: IMU hybridization with a multi-beam telemeter and an atomic gravimeter in a centralized data fusion architecture.

This matrix expression (19) shows, compared to equation (17), that gravimetry contributes to the observability of the following states:

- Position information is enhanced by complementary positive terms depending on the local gravity field gradient $(\nabla_g^x, \nabla_g^y)^T$;
- x-axis velocity information becomes explicitly observable;
- Non diagonal terms bring cross information that will benefit to the whole state estimation.

All non-zero diagonal terms of the bathymetric Fisher information matrix are enhanced with positive (square) terms. These terms represent the theoretical impact of sensor fusion on expected estimation accuracy.

y-axis and z-axis velocities information remains the same, i.e., only depending on indirect estimation via information brought by the dynamics. A significant improvement is then expected on position estimation and x-axis velocity estimation. The estimation error reduction of these variable may also benefit to the others velocities estimation accuracy. Furthermore, atomic gravimeter offers a very low level noise σ_g [3], which increases the impact of the gravimeter's contribution to information (proportional to $\frac{1}{\sigma_g^2}$).

The next section illustrates these theoretical aspects with numerical simulations.

IV. Simulation example

The reference trajectory is located in an ambiguous area of the map (see Fig. 6). The spatial resolution of the bathymetric map is about $200\,\mathrm{m}$. The gravimetric map has a spatial resolution of about $2000\,\mathrm{m}$. Measurements and predicted measurements of the filters are obtained by bilinear interpolations.

A. State-space model

The vehicle state x is comprised of the position p and the velocity v, where $p = [p^x, p^y, p^z]^\top$ is expressed in meter and $v = [v^x, v^y, v^z]^\top$ is expressed in meter per second. The state dynamical model is written in the following discrete way:

$$x_k = \begin{bmatrix} p_k \\ v_k \end{bmatrix} = \begin{pmatrix} \mathbf{I}_3 & \Delta_k\, \mathbf{I}_3 \\ \mathbf{0}_3 & \mathbf{I}_3 \end{pmatrix} x_{k-1} + \eta_k \qquad (20)$$

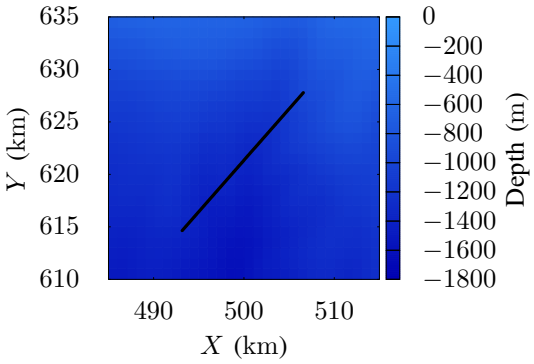

Fig. 6: Bathymetric map of the California coast with the true trajectory.

where $\mathbf{I}_3$ and $\mathbf{0}_3$ are respectively the identity matrix and the zeros matrix of dimension 3 by 3, Δ_k is the discretization time-step and η_k a Gaussian process noise i.i.d. of covariance matrix Q_k. Equation (20) models in a simplified way the position drift of an AUV Inertial Measurement Unit (IMU) that would start with a position and velocity error (alignment error) and a negligible velocity drift. This approximation is meaningful when the IMU gyrometers are sufficiently accurate for short duration scenarios.

The measurement equation is given by:

$$y_k = \begin{bmatrix} \sqrt{(p_k^x - p_{1,k}^x)^2 + (p_k^y - p_{1,k}^y)^2 + (p_k^z - \mathrm{map}_{\mathrm{mb}}(p_{1,k}^x, p_{1,k}^y))^2} \\ \vdots \\ \sqrt{(p_k^x - p_{m,k}^x)^2 + (p_k^y - p_{m,k}^y)^2 + (p_k^z - \mathrm{map}_{\mathrm{mb}}(p_{m,k}^x, p_{m,k}^y))^2} \\ a\ p_k^y + b\ p_k^z + c\ v_k^x + \mathrm{map}_{\mathrm{ga}}(p_k^x, p_k^y) \end{bmatrix} + \begin{bmatrix} \nu_{1,k} \\ \vdots \\ \nu_{m,k} \\ \nu_k{}' \end{bmatrix} \qquad (21)$$

where $\nu_{i,k}$ and $\nu_k{}'$ are assumed to be white Gaussian noises.

In the present application, the choice of the A2BC kernel in the A2BC-RPF is a Cauchy kernel, whose scale parameter is adaptively determined online (12). To compare the filters, a Cauchy kernel with constant scale parameter is chosen for the RPF likelihood.

B. Comparison criteria

Comparisons are done using the following criteria evaluated for $N_{mc} \in \mathbb{N}^*$ Monte Carlo runs.

- The Root Mean Square Error (RMSE) of filters:

$$\text{RMSE}_k^x = \sqrt{\frac{\sum_{i=1}^{N_{mc}} ||\hat{x}_k^i - x_k||_2^2}{N_{mc}}} \tag{22}$$

where $\hat{x}_k^i$ is the state estimate for the i^{th} Monte Carlo simulation. The RMSE of the horizontal position is calculated as follows:

$$\text{RMSE}_k^{p_h} = \sqrt{\text{RMSE}_k^{p^x\,2} + \text{RMSE}_k^{p^y\,2}} \tag{23}$$

The horizontal velocity is computed as above by replacing p_k by v_k, p^x by v^x and p^y by v^y.

- The number of non-convergent runs:
The filter is said to not converge if, at the end of the trajectory, during the last 5 consecutive measurement time-steps, the state estimate $\hat{x}_k$ leaves the confidence ellipsoid Γ_k given by the covariance $\hat{P}_k$, such that

$$\Gamma_k = \left\{ x_k | (x_k - \hat{x}_k)^T \hat{P}_k^{-1} (x_k - \hat{x}_k) \leq \alpha_{\text{th}}^2 \right\} \tag{24}$$

where the threshold α_{th} is such that $\mathbb{P}(\mathcal{X}^2(d) \leq \alpha_{\text{th}}^2) = 0.99$ with d the dimension of the state vector and $\mathcal{X}^2$ the Chi-squared distribution.

C. Navigation scenarios

The simulation parameters are summarized in Table I.

TABLE I: Simulation configuration.

Stace-space model parameters	Value
Number of Monte Carlo runs	100
Sampling period	$\Delta_k = 1$ s
Number of bathymetric measurements	600
Number of gravimetric measurements	40
Trajectory duration	10 min
Number of beams	$m = 5$
Number of particles	$N = 1000$
Resampling threshold	$N_{th} = 0.75\ N$
Regularization bandwidth parameter	$\mu = 0.3$
Initial position	$[110000, 140000, -100]^\top$ m
Initial velocity	$[5, 5, 0.05]^\top$ m s^{-1}
Initial uncertainty in position (st.d.)	$[1000, 1000, 100]$ m
Initial uncertainty in velocity (st.d.)	$[0.5, 0.5, 0.05]$ m s^{-1}
Process noise in position (st.d.)	$[3, 3, 0.3]$ m
Process noise in velocity (st.d.)	$[0.015, 0.015, 0.0015]$ m s^{-1}
Measurements	
Error of each beam range (st.d.)	$\sigma_{mb} = 10$ m
Gravimeter error (st.d.)	$\sigma_{ga} = 0.3$ mGal
A2BC parameter	
Domain of the bandwidth parameter	$\mathcal{D} = [1 : 0.5 : 5]$

Fig. 7 shows the position RMSEs for both filters using the simulation conditions described above. The velocity RMSEs are illustrated in Fig. 8 and Fig. 9. Only convergent Monte Carlo runs are used to plot the RMSEs curves. The number of non-convergent runs for each filter is provided in Fig. 10.

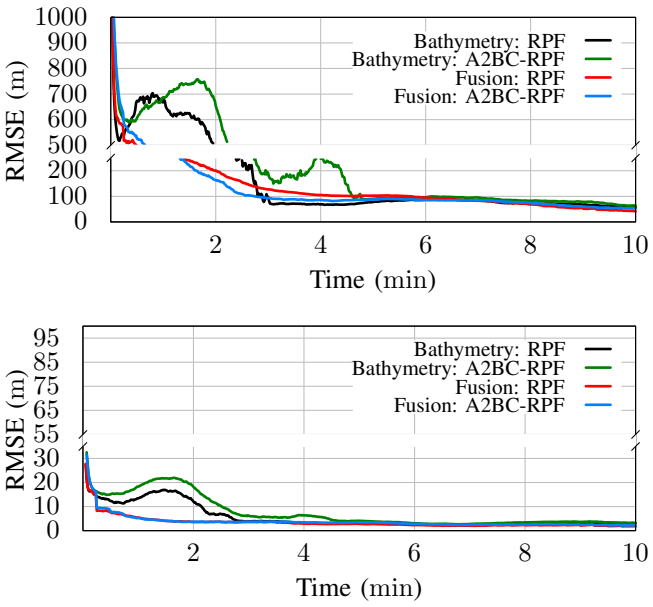

Fig. 7: Plot of the RMSEs for the horizontal (upper plot) and vertical position (lower plot). "Bathymetric" corresponds to the bathymetric-aided navigation and "Fusion" to the bathymetry and gravimetry fusion scenario.

In Fig. 7 and Fig. 8, the RMSEs curves decrease with time for both the simple bathymetry, and the bathymetry and gravimetry fusion scenarios. Overall, the RMSEs curves in the fusion scenario (red and blue curves) are lower than in the bathymetric situation (black and green curves). The fusion strategy presented in Section III-D improves the quality of filter estimates. We note a significant difference between the RMSEs curves of the horizontal velocity in Fig. 8 which is due to the presence of the x-axis velocity directly in the measurement equation (3) and can be observed in Fig. 9 for the RPF.

The A2BC-RPF increases the accuracy of the filter estimates. This is particularly visible on the figures in the case of sensor fusion. For the bathymetric scenario, the A2BC-RPF RMSEs curves are higher than the RPF RMSEs curves. This is due to the removal of non-convergent runs (see Fig. 10). Still in the bathymetric scenario, we observe on the position RMSEs curves the presence of jumps around 1.5 s and 4 s. These jumps are due to the ambiguity of the navigation trajectory. Since A2BC filters waits until the terrain is more informative to remove the ambiguity, it is normal to observe more jumps at the beginning of the trajectory than classic filters. A2BC filters are therefore more robust as shown by the diminution of the number of non-convergent runs in Fig. 10.

For 100 Monte Carlo runs, the number of non-convergences is shown in Fig. 10. Overall, fewer non-convergent runs are observed when the multi-beam telemeter is fused to the gravimeter. Indeed, for the RPF, the number of non-convergent runs decreases from 16 to 9 with the gravimeter fusion. A decrease is also observed for the A2BC-RPF: the number of non-convergent runs drops from 5 to 3. A significant decrease

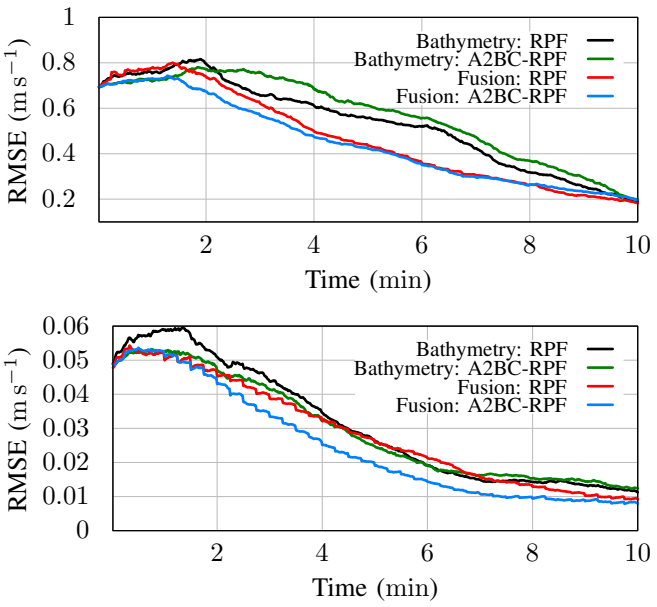

Fig. 8: Plot of the RMSEs for the horizontal (upper plot) and vertical velocity (lower plot). "Bathymetric" corresponds to the bathymetric-aided navigation and "Fusion" to the bathymetry and gravimetry fusion scenario.

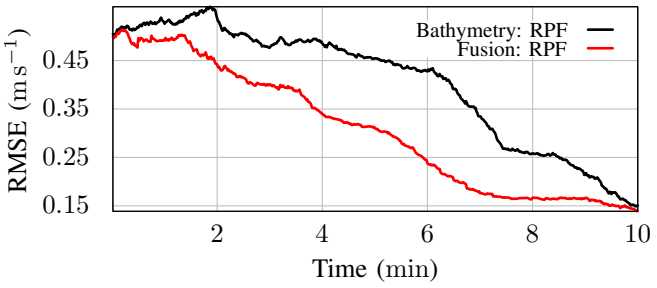

Fig. 9: Plot of the RMSEs for the velocity on the x-axis. "Bathymetric" corresponds to the bathymetric-aided navigation and "Fusion" to the bathymetry and gravimetry fusion scenario.

in the number of non-convergent runs was expected as the A2BC method optimizes the impact of the weights correction.

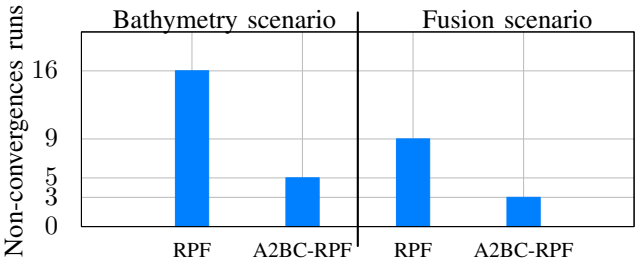

Fig. 10: Histogram of the number of non-convergences for 100 Monte Carlo runs.

V. Conclusion

This paper focuses on a sensor fusion strategy between a multi-beam telemeter and an atomic gravimeter, in an underwater terrain-aided navigation application. We demonstrated that the multi-beam telemeter and gravimeter fusion provides more accurate estimates through the direct observation of the x-axis velocity in the gravimeter measurement equation. The A2BC filters are more robust to nonlinearities and measurement ambiguities than classical filters, as the number of non-convergences is significantly reduced. Bathymetry and gravimetry fusion by A2BC particle filters is thus a promising way to perform embedded underwater navigation.

References

[1] C. Musso, N. Oudjane and F. Le Gland. "Improving regularised particle filters". In: *Sequential Monte Carlo methods in practice, Springer*. 2001, pp. 247-271.

[2] J. Melo and A. Matos. "Survey on advances on terrain based navigation for autonomous underwater vehicles". In: *Ocean Engineering*. Vol.139, 2017, pp. 250-264.

[3] Y. Bidel, O. Carraz, R. Charrière, M. Cadoret, N. Zahzam and A. Bression. "Compact cold atom gravimeter for field applications". In: *Applied Physics Letters*. Vol.102, no.14, 2013, pp. 144107.

[4] B.D.O. Anderson and J.B. Moore. "Optimal filtering". Prentice Hall, Englewood Cliffs, N.J. USA, 1979.

[5] P. Del Moral. "Nonlinear Filtering: Interacting Particle Resolution". In: *Markov Processes and Related Fields*. Vol.2, no.4, 1996, pp. 555-580.

[6] C. Palmier, K. Dahia, N. Merlinge, P. Del Moral, D. Laneuville and C. Musso. "Adaptive Approximate Bayesian Computational Particle Filters for Underwater Terrain Aided Navigation". In: *22nd International Conference on Information Fusion*. 2019.

[7] T. Li, M. Bolic and P.M. Petar. "Resampling methods for particle filtering: classification, implementation, and strategies". In: *IEEE Signal processing magazine*. Vol.32, no.3, 2015, pp. 70-86.

[8] P. Del Moral, A. Doucet and A. Jasra. "On Adaptive Resampling Procedures for Sequential Monte Carlo Methods". In: *Bernoulli*. Vol.18, no.1, 2012, pp. 252-278.

[9] A. Kong, J.S. Liu and W.H. Wong. "Sequential imputations and Bayesian missing data problems". In: *Journal of the American statistical association*. Vol.89, no.425, 1994, pp. 278-288.

[10] A. Doucet, S. Godsill and C. Andrieu. "On sequential Monte Carlo sampling methods for Bayesian filtering". In: *Statistics and computing, Springer*. Vol.10, no.3, 2000, pp. 197-208.

[11] P. Del Moral, J. Jacod and P. Protter. "The Monte-Carlo method for filtering with discrete-time observations". In: *Probability Theory and Related Fields*. Vol.120, 2001, pp. 346-368.

[12] J.M Marin, P. Pudlo, C.P. Robert and R.J. Ryder. "Approximate Bayesian computational methods". In: *Statistics and Computing*. Vol.22, 2012, pp. 1167-1180.

[13] D. K. Meduna. "Terrain relative navigation for sensor-limited systems with application to underwater vehicles". In: *Stanford University*. 2011.

[14] Ch. J. Bordé. "Atomic interferometry with internal state labelling". In: *Physics letters A*. Vol. 140, no. 1-2, 1989, pp. 10-12.

[15] J. F. Clauser. "Ultra-high sensitivity accelerometers and gyroscopes using neutral atom matter-wave interferometry". In: *Physica B+ C*. Vol. 151, no. 1-2, 1988, pp. 262-272.

[16] C. Musso, B. Sacleux, A. Bresson, J.-M. Allard, K. Dahia, Y. Bidel, N. Zahzam and C. Palmier. "Terrain-aided navigation with an atomic gravimeter". In: *2019 22th International Conference on Information Fusion (FUSION)*. 2019, pp. 1-8.

[17] B. Grocholsky. "Information-theoretic control of multiple sensor platforms". In: *University of Sydney. School of Aerospace, Mechanical and Mechatronic*. 2002.

[18] F. C. Teixeira, J. Quintas, P. Maurya and A. Pascoal. "Robust particle filter formulations with application to terrain-aided navigation". In: *International journal of Adaptive control and signal processing*. Vol. 31, no. 4, 2017, pp. 608-651.

[19] E. L. Lehmann and G. Casella. "Theory of point estimation". In: *Springer Science & Business Media*. 2006.

[20] B. Ristic, S. Arulampalam and N. Gordon. "Beyond the Kalman filter: Particle filters for tracking applications". In: *Artech house*. 2003.